PHYSICAL REVIEW B **90**, 201107(R) (2014)

Supercoupling of surface waves with ϵ-near-zero metastructures

Yue Li[1,2] and Nader Engheta[2,*]

[1]*Department of Electrical Engineering, Tsinghua University, Beijing 100084, China*

[2]*Department of Electrical and Systems Engineering, University of Pennsylvania, Philadelphia, Pennsylvania 19104, USA*

(Received 12 August 2014; revised manuscript received 10 October 2014; published 13 November 2014)

It is known that ϵ-near-zero (ENZ) structures may provide exciting possibilities for light-matter interaction, including the phenomenon of supercoupling, i.e., channeling of wave energy through ultranarrow conduits connecting two waveguides. Here, we extend this concept to the surface waves using structures with effective ENZ properties, exploring how surface waves can tunnel through such structures with essentially no reflection, even in the presence of sharp bends. Such ENZ metastructures support tunneling of waves with longitudinal wave numbers near zero. The surface waves may include examples of transverse electric (TE) surface waves along the grounded dielectric slabs (e.g., in the microwave regime) and TE surface-plasmon polariton waves along the negative-permeability interfaces. The ENZ metastructures can transfer the surface wave energy from one side to another by an anomalous squeezing effect, which is effectively independent of the length and the shape of the ENZ metastructures. The interaction of electromagnetic waves with such systems offers exciting possibilities for the design of flat photonic devices and components.

DOI: 10.1103/PhysRevB.90.201107 PACS number(s): 78.66.Sq, 42.82.Et, 52.40.Db, 52.40.Fd

The field of metamaterials, i.e., engineered materials and structures with tailorable electric (ϵ) and/or magnetic (μ) properties, has attained considerable attention in the scientific and engineering communities from the microwave to the optical regimes. In particular, the class of metamaterials named ϵ-near-zero (ENZ) metamaterials in which the relative permittivity attains near-zero values around a certain frequency has become an important topic due to their anomalous properties in wave propagating and scattering [1,2]. In ENZ metamaterials, we can approximately "loosen" the connection between the spatial features (related to wavelength λ) from the temporal features (related to frequency f), e.g., one can achieve a long wavelength for a high-frequency signal. The ENZ materials and structures can be obtained via several approaches, e.g., in some available materials with Drude dispersion, such as transparent conducting oxides, such as indium tin oxide, near their plasma frequencies in near-infrared (NIR) wavelength [3,4], via engineering synthesis, e.g., stacking thin layers of pairs of positive- and negative-permittivity materials [5,6], and by using a metallic waveguide operating near its cutoff frequency [7,8]. The ENZ structures provide several interesting phenomena, e.g., electric-field enhancement [9], light funneling [10], coherent perfect absorption [11], and the supercoupling effect [7,8,12–14], among others. In particular, the original supercoupling was for the energy squeezing and tunneling through ultranarrow conduits connecting the waveguides, a phenomenon which has been theoretically and experimentally studied in Refs. [7,8,12–14]. In such ENZ channels, the wave exhibits an effectively "infinite" phase velocity, essentially propagating in a "static" manner with almost no reflection losses, regardless of the shape and the length of the channel as long as the channel is kept very narrow. These features have offered interesting characteristics and potential applications in Purcell enhancement of molecular emissions [15], nonlinear control of fields and waves [16], displacement-current conduits [17], and dielectric sensing [18], just to name a few.

Here, we extend the ENZ-based supercoupling concept into the paradigm of surface waves and metasurfaces [19–24] using structures along which the longitudinal wave number of the surface wave may be near zero. In the literature [25], the surface wave is studied in an anisotropic ENZ (AENZ) metamaterial, e.g., an anisotropic material with only one component of the permittivity tensor being zero for the purpose of perfect bending. However, in such a scenario the field is not uniformly distributed in the region of AENZ metamaterials, and the operating frequency is highly dependent on the geometry. Different from Ref. [25], here we demonstrate how the ENZ metastructures can transfer the surface wave energy from one side to another by an anomalous supercoupling effect with essentially no reflection losses, which is also effectively independent of the length and the shape of these thin structures. We theoretically study two examples of the proposed supercoupling of surface waves: (1) the transverse electric (TE) surface waves along the grounded dielectric slabs, which are common in the microwave regime and (2) the TE surface-plasmon polariton (SPP) waves along the magnetic-material-dielectric interfaces. We assume the $e^{-i\omega t}$ time convention, where ω is the angular frequency.

To begin, we first describe the generic structure of the ENZ metastructure. Consider a surface wave propagating along the interface of two media with permittivity values of ϵ_1 and ϵ_2 as sketched in Fig. 1(a). In order to achieve an ENZ metastructure with a zero longitudinal component of the wave number on a typical surface, a top conductor and a filling medium are utilized and positioned on the surface [middle part of Fig. 1(a)]. The top conductor is assumed to be a perfect electric conductor (PEC), and the medium filling the region between the top conductor and the surface has permittivity $\epsilon_{\rm ms} > 0$. To achieve a zero longitudinal wave number ($k_z = 0$) along the interface of the filling medium and the surface in the middle section, the wave number in the filling medium has to have only the transverse component (k_x). In this situation, the surface wave is no longer evanescent in the transverse direction, and thus

*Author to whom correspondence should be addressed: engheta@ee.upenn.edu

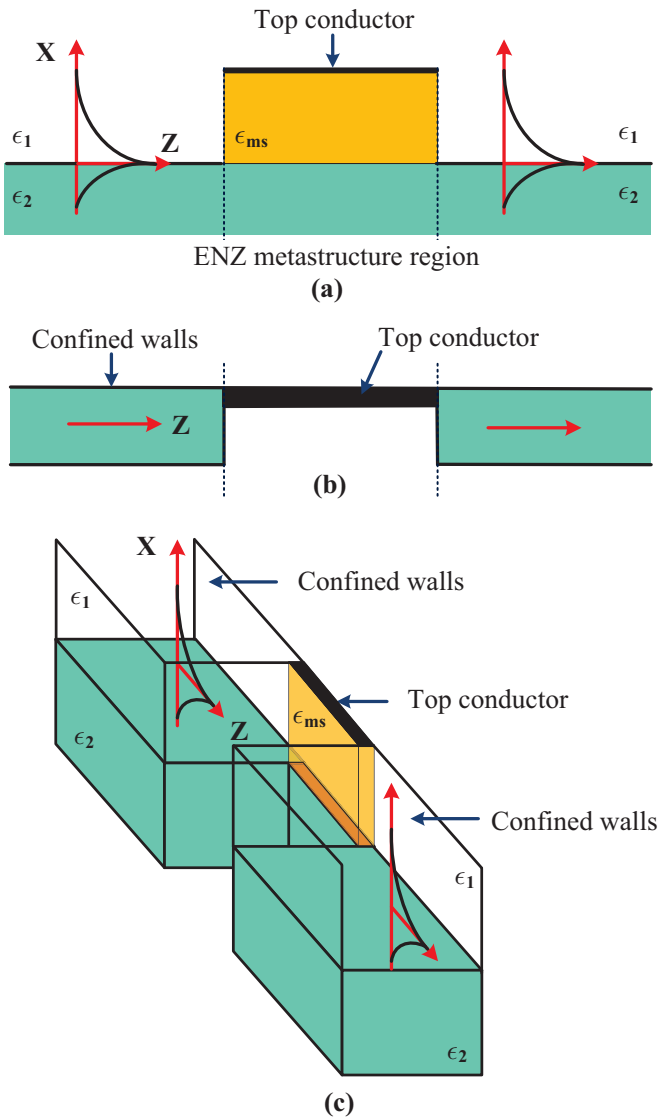

FIG. 1. (Color online) Generic geometry of a surface wave propagating along the surface with an ENZ metastructure region in the middle. (a) Side view. The ENZ metastructure region in the middle between the two regions 1 and 2 are in the same plane. (b) and (c) Top and perspective views. The ENZ metastructure region has the narrow shape. The surface wave in this region is confined by the PEC lateral confined walls and top ceiling.

the surface wave may "leak" into the open space. To prevent such leakage, as shown in the top and perspective views of Figs. 1(b) and 1(c), the ENZ metastructure is surrounded by the PEC side walls and top ceiling. Similar to the case of ENZ supercoupling in Refs. [2,12,13] and for the purpose of matching, here we also make the ENZ region have a narrow shape as shown in Figs. 1(b) and 1(c). Since the side walls and the ceiling of the metastructure region are assumed to be PEC, the surface wave is forced to tunnel in the z-axis direction.

As the first example, we examine the operating principle of an ENZ metastructure for the TE surface wave along the PEC-grounded dielectric waveguide. A TE surface wave propagates along the PEC-grounded dielectric slab as shown in Fig. 2(a). The wave is confined in the dielectric slab positioned above the PEC ground plane. Above the dielectric slab is free space with a permittivity ϵ_0 and a thickness of $h = 15$ mm. The surface wave is evanescent in the transverse direction in the free space, and the top PEC ceiling in this section does not play an important role since the evanescent part of the surface wave does not reach appreciably to the PEC ceiling. The dispersion relation of the TE surface wave along the PEC-grounded dielectric slab is expressed as [26]

$$\tan\left(d\sqrt{\omega^2\epsilon_1\mu_0-\beta^2}\right)+\sqrt{\omega^2\epsilon_1\mu_0-\beta^2}/\sqrt{\beta^2-\omega^2\epsilon_0\mu_0}=0, \tag{1}$$

where β is the longitudinal wave number of the TE surface wave. We use PEC side walls as a waveguide to confine the TE surface wave propagating along the z axis. The grounded dielectric is with the permittivity $\epsilon_1 = 10\,\epsilon_0$ and the width $w = 10$ mm. The height of the waveguide in the x direction is 20 mm, and the thickness of the dielectric slab is $d = 5$ mm.

In the ENZ metastructure section as shown in Figs. 2(b) and 2(c), we need to have a structure that can provide a near-zero longitudinal wave number for the guided wave, i.e., to have a waveguide operating near its cutoff frequency. To achieve this, instead of adding another dielectric layer with ϵ_{ms} on top of the grounded substrate as depicted in the generic Fig. 1, we choose to have the grounded dielectric to have the permittivity $\epsilon_{ms} = 4\,\epsilon_0$ and the region above this substrate to be free space bounded by the top PEC ceiling. The length and the width of this section are $l_{ch} = 30$ and $w_{ch} = 0.1$ mm, respectively. The ENZ section is a uniform U-shaped transition channel, similar to the case in Refs. [2,12,13], which is used for impedance matching between the surface wave region and the ENZ region.

As seen from Fig. 2(b), strong electric-field intensity is present in the ENZ metastructure, which is confined by top, bottom, and side PEC conductors. Along the longitudinal axis in the ENZ region, the electric field has a uniform phase since this section is functioning as a waveguide near its cutoff frequency and consequently $k_z = 0$. Therefore, it effectively behaves as an ENZ structure. For this section, the dispersion relationship is given below to achieve the zero longitudinal wave number by choosing the proper value of ϵ_{ms} for a given set of values for ω, d, and h,

$$\tan(h\sqrt{\omega^2\epsilon_0\mu_0})/\sqrt{\epsilon_0}+\tan(d\sqrt{\omega^2\epsilon_{ms}\mu_0})/\sqrt{\epsilon_{ms}}=0. \tag{2}$$

Figure 2 presents our simulation results using the commercial simulator CST MICROWAVE STUDIO® [27]. First, we examined the operating frequencies for the ENZ metastructure tunneling for different lengths of the ENZ section. When l_{ch} = 30 mm, the ENZ operating frequency is 6.341 GHz with nearly total transmission and zero reflection. In Figs. 2(b) and 2(c), we show the simulation results for the electric-field distribution. The TE surface wave is indeed confined in the ENZ metastructure region with a uniform phase and highly enhanced magnitude along the region. We also calculate analytically the related parameters using the dispersion relation given in Eq. (2) and compare them with the simulation results. For example, we calculate the value of the required ϵ_{ms} at the ENZ operating frequency of 6.341 GHz to be 3.987 ϵ_0, which agrees well with $\epsilon_{ms} = 4\,\epsilon_0$ we used in the simulation. When l_{ch} = 60 and 90 mm, the ENZ operating frequencies are 6.354 and 6.359 GHz,

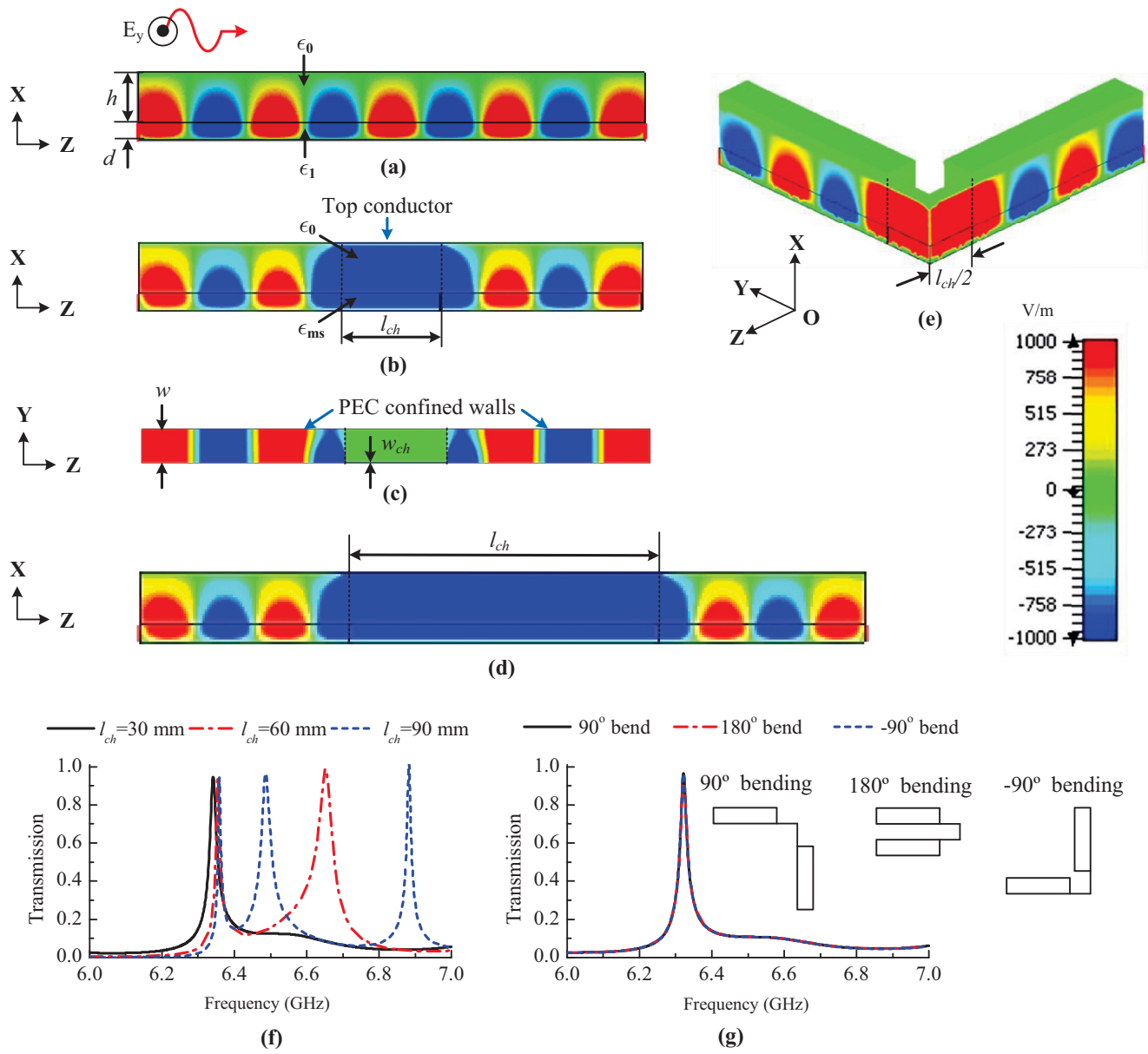

FIG. 2. (Color online) TE surface wave in the PEC-grounded dielectric, squeezing along the ENZ metastructure region. (a) Side view of TE surface wave without the ENZ section present. (b) Side view of electric-field distributions in the grounded dielectric slab at 6.341 GHz. The ENZ region is an $l_{ch} = 30$-mm straight channel. (c) Top view of (b), the lateral confined walls and the ceiling are PEC conductors. (d) Side view of electric-field distributions of ENZ metastructure with an $l_{ch} = 90$-mm straight channel at 6.359 GHz. (e) Three-dimensional (3D) view of the electric-field distributions of the ENZ metastructure with an $l_{ch} = 30$-mm and a $-90°$ bent channel at 6.322 GHz. Transmission coefficient magnitudes for tunneling through the ENZ region (f) straight channel with a different length and (g) with $l_{ch} = 30$ mm but different bending angles.

respectively. In Fig. 2(f), we present the transmission coefficient as a function of frequency for different lengths of the ENZ metastructure section. The ENZ operating frequencies are almost unchanged for different lengths with the transmission coefficient to be unity at the ENZ operating frequency, similar to the effect in the bulk structure [2,12,13]. We also obtain the Fabry-Pérot (FP) unity transmission, which unlike the ENZ tunneling is highly dependent on the physical length. The electric-field distribution at the ENZ frequency for the case of $I_{ch} = 90$ mm is shown Fig. 2(d). The distribution is almost the same as Fig. 2(b) but with a three times longer ENZ metastructure region. As in the case of the ENZ bulk structure in Ref. [2], this anomalous squeezing effect for the metasurface scenario is effectively independent of the length.

Another important property of the ENZ metastructure is the surface wave supercoupling in the presence of sharp bends. We have simulated three different bent structures, including 90°, 180°, and $-90°$ bends. The transmission coefficient magnitudes are depicted in Fig. 2(g). In all these cases, the surface wave is tunneled at 6.322 GHz with no reflection. We show

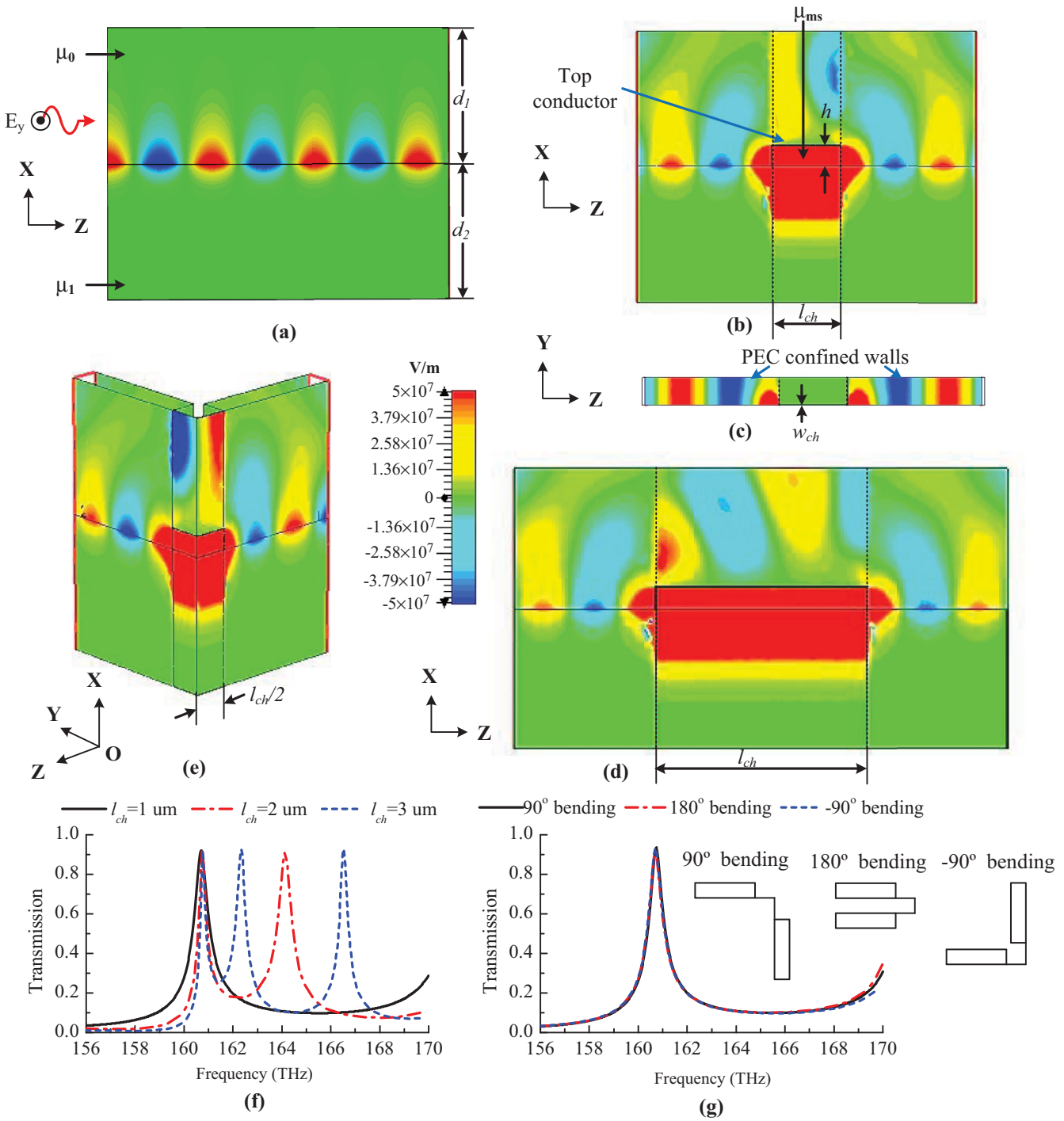

FIG. 3. (Color online) TE SPP squeezing along the ENZ metastructure with the negative-permeability substrate. (a) Side view of the TE SPP without the ENZ section present. (b) Side view of electric-field distributions in an air-magnetic-material interface at 160.70 THz. The ENZ region is an $l_{ch} = 1$-μm straight channel. (c) Top view of (b), the lateral confined walls and the ceiling are PEC conductors. (d) Side view of the electric-field distributions of the ENZ metastructure with an $l_{ch} = 3$-μm straight channel at 160.72 THz. (e) A 3D view of the electric-field distributions of the ENZ metastructure with an $l_{ch} = 1$-μm bent channel at 160.72 THz. Transmission coefficient magnitudes for the ENZ metastructure (f) straight channel with a different length and (g) with $l_{ch} = 1$ μm but different bending angles.

the simulation results for the electric-field distribution with a $-90°$ bend in Fig. 2(e) where the two surface wave regions are connected by a $-90°$ bent ENZ metastructure. In this region, the electric-field distribution is the same as the straight ones in Figs. 2(b) and 2(d) with an almost uniform phase.

As the second example, we extend the concept of an ENZ metastructure to the case of a TE SPP for the interface between the free space and the negative-permeability materials. In order to compare with the first example, here we maintain the PEC boundary and TE surface wave. Therefore, we choose

magnetic materials to support the TE SPP. The methodology can also be adopted in the study of a TM SPP using the negative-permittivity materials. As is well known, the bending of SPP beams results in high reflection loss [28,29]. Supercoupling of the SPP using our proposed metastructure may offer a potential solution to alleviate this problem. As shown in Fig. 3(a), the interface for SPP propagation is composed of free space with permeability of μ_0 and permittivity of ϵ_0 and the magnetic material with permeability of μ_1. The longitudinal wave number of the TE SPP is $\beta = \omega\sqrt{\epsilon_0(\mu_0\mu_1)/(\mu_0+\mu_1)}$. In the transverse plane, the wave is evanescent in both upper and lower magnetic materials. Although the permeability usually follows the Lorentzian dispersion, here without loss of generality and for the sake of simplicity, we use the Drude model to describe the dispersion of the permeability of this medium with $\mu_1 = \mu_0[\mu_\infty - \omega_p^2/\omega(\omega + i\gamma)]$ where we assume the parameters $\omega_p = 2.65 \times 10^{15}$rad/s, $\mu_\infty = 3.91$, and $\gamma = 0$ to ignore the loss at first. The thickness of the magnetic layer is $d_2 = 2.4$ μm. The side confining walls are assumed to be a PEC with a height of $d_1 + d_2 = 2.4 + 2.4 = 4.8$ μm, separated with 0.4 μm. We have no PEC ceiling and ground in this section. As depicted in Fig. 3(b), the ENZ metastructure region, which is the interface between the magnetic substrate μ_1 mentioned above and another magnetic material with permeability $\mu_{\rm ms} > 0$, has a narrow width of 0.01 μm with the length $l_{\rm ch}$ of 1 μm, PEC side walls, and a PEC ceiling. A superstrate $\mu_{\rm ms}$ is used between the medium μ_1 and the PEC top conductor, and its thickness h is 0.6 μm. This section is also U shaped for modes matching purposes. The SPP propagates along the z axis, and the electric vector is mostly oriented along the y axis.

As shown in the simulation results in Fig. 3(b), here we have analogous field distribution along the ENZ metastructure with a zero longitudinal wave number. We see that the electric field is uniformly distributed along the direction of surface wave tunneling. Compared with the ENZ metastructure in the first example, here the bottom PEC ground plane has been removed since the wave penetrating into the magnetic material with μ_1 is evanescent due to the negative permeability. The dispersion relationship required to achieve the zero longitudinal wave number in the ENZ region can be expressed as

$$2h\sqrt{\omega^2\mu_{\rm ms}\epsilon_0} + \arctan[2\sqrt{\mu_{\rm ms}|\mu_1|}/(|\mu_1| - \mu_{\rm ms})] = \pi. \quad (3)$$

Using the CST MICROWAVE STUDIO® [27], we have found the ENZ operating frequency to be 160.70 and 160.72 THz for the structure with the lengths of 1 and 3 μm, respectively. The electric-field distributions for these cases are shown in Figs. 3(b)–3(d). The TE SPP is seen to be confined in the ENZ metastructure region with a uniform phase distribution and enhanced magnitude. We also show the magnitude of the transmission coefficient vs frequency with different lengths of the ENZ region in Fig. 3(f). As in the first example, here we also see the FP modes appear and shift to the lower band with longer $l_{\rm ch}$ for the ENZ metastructure. But the ENZ operating frequencies for different lengths of 1–3 μm remain almost unchanged. We also calculated the value of required $\mu_{\rm ms}$ using dispersion Eq. (3) at 160.70 THz and obtained it to be 1.002 μ_0 with good agreement with the air superstrate with $\mu_{\rm ms} = 1$ μ_0.

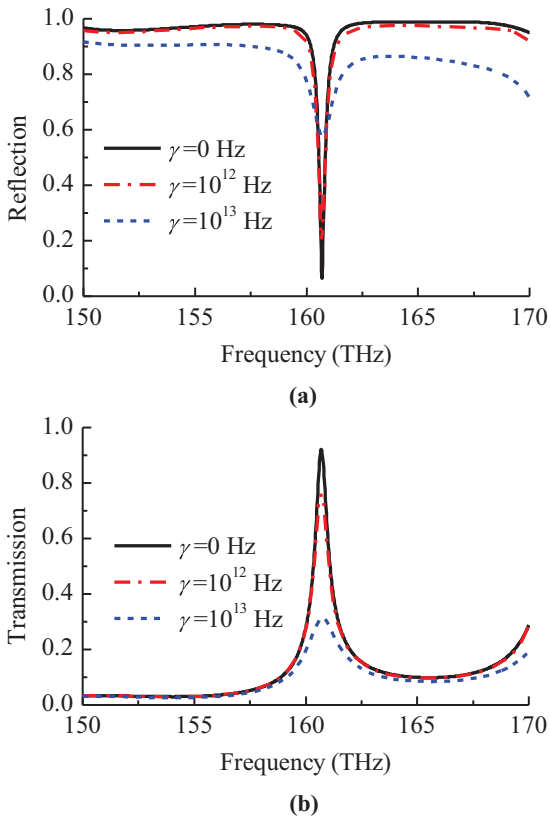

FIG. 4. (Color online) (a) Reflection and (b) transmission coefficient magnitudes for supercoupling of surface waves with different collision frequencies in the Drude model of the permeability of the substrate.

We also examined the ENZ tunneling effect with different bent structures. Figure 3(e) shows the electric-field distributions in the $-90°$ bend at the ENZ operating frequency of 160.72 THz. The input electric field is y polarized, and the output electric field is z polarized. We plotted the transmission coefficient magnitude for the three bent structures in Fig. 3(g). The ENZ metastructure can transfer the SPP from one side to another with almost total transmission, effectively independently of the shape.

Finally, the role of loss is also studied. We change the collision frequency γ in the Drude model for the permeability of the substrate μ_1 in order to explore the effect of the material's loss on the ENZ metastructure response. As illustrated in Fig. 4, using the numerical simulation we evaluated the reflection and transmission coefficient magnitudes for the cases of $\gamma = 0$ Hz (imaginary part of μ is 0), $\gamma = 10^{12}$ Hz (imaginary part of μ is 0.0068 μ_0), and $\gamma = 10^{13}$ Hz (imaginary part of μ is 0.0682 μ_0). The reflection increases, and the transmission decreases with larger values of γ. However, the ENZ supercoupling effect with $\gamma = 10^{13}$ Hz still exists with a somewhat similar electric-field distribution in the ENZ metastructure region as shown in Fig. 3(b). But on the input side, we do see some partial standing wave due to the nonzero reflection.

In conclusion, we have extended the concept of ENZ supercoupling to the surface waves with the analogous

effects including no reflection loss, tunneling along the ENZ metastructure with arbitrary channel shapes and lengths. This phenomenon suggests potential applications in engineering flat photonic devices and components with unconventional properties.

This work was supported in part by the U.S. Office of Naval Research (ONR) Multidisciplinary University Research Initiative (MURI) Grant No. N00014-10-1-0942 and in part by the National Natural Science Foundation of China under Contract No. 61301001 to Y. Li.

[1] N. Engheta, Science **340**, 286 (2013).
[2] M. G. Silveirinha and N. Engheta, Phys. Rev. Lett. **97**, 157403 (2006).
[3] J. Kim, G. V. Naik, N. K. Emani, U. Guler, and A. Boltasseva, IEEE J. Sel. Top. Quantum Electron. **19**, 4601907 (2013).
[4] A. Boltasseva and H. A. Atwater, Science **331**, 290 (2011).
[5] A. Alu and N. Engheta, Phys. Rev. Lett. **103**, 143902 (2009).
[6] R. Maas, J. Parsons, N. Engheta, and A. Polman, Nat. Photonics **7**, 907 (2013).
[7] E. J. R. Vesseur, T. Coenen, H. Caglayan, N. Engheta, and A. Polman, Phys. Rev. Lett. **110**, 013902 (2013).
[8] B. Edwards, A. Alù, M. E. Young, M. Silveirinha, and N. Engheta, Phys. Rev. Lett. **100**, 033903 (2008).
[9] S. Campione, D. de Ceglia, M. A. Vincenti, M. Scalora, and F. Capolino, Phys. Rev. B **87**, 035120 (2013).
[10] D. C. Adams, S. Inampudi, T. Ribaudo, D. Slocum, S. Vangala, N. A. Kuhta, W. D. Goodhue, V. A. Podolskiy, and D. Wasserman, Phys. Rev. Lett. **107**, 133901 (2011).
[11] S. Feng and K. Halterman, Phys. Rev. B **86**, 165103 (2012).
[12] M. G. Silveirinha and N. Engheta, Phys. Rev. B **76**, 245109 (2007).
[13] A. Alu, M. G. Silveirinha, and N. Engheta, Phys. Rev. E **78**, 016604 (2008).
[14] A. Alu and N. Engheta, Phys. Rev. B **78**, 035440 (2008).
[15] A. Alu and N. Engheta, Phys. Rev. Lett. **103**, 043902 (2009).
[16] D. A. Powell, A. Alu, B. Edwards, A. Vakil, Y. S. Kivshar, and N. Engheta, Phys. Rev. B **79**, 245135 (2009).
[17] B. Edwards and N. Engheta, Phys. Rev. Lett. **108**, 193902 (2012).
[18] A. Alu and N. Engheta, Phys. Rev. B **78**, 045102 (2008).
[19] N. Yu, P. Genevet, M. A. Kats, F. Aieta, J. Tetienne, F. Capasso, and Z. Gaburro, Science **334**, 333 (2011).
[20] N. Engheta, Science **334**, 317 (2011).
[21] F. Monticone, N. M. Estakhri, and A. Alu, Phys. Rev. Lett. **110**, 203903 (2013).
[22] G. Gok and A. Grbic, Phys. Rev. Lett. **111**, 233904 (2013).
[23] A.V. Kildishev, A. Boltasseva, and V. M. Shalaev, Science **339**, 1289 (2013).
[24] C. L. Holloway, E. F. Kuester, J. A. Gordon, J. O'Hara, J. Booth, and D. R. Smith, IEEE Antennas Propag. Mag. **54**, 10 (2012).
[25] J. Luo, P. Xu, H. Chen, B. Hou, L. Gao, and Y. Lai, Appl. Phys. Lett. **100**, 221903 (2012).
[26] D. M. Pozar, *Microwave Engineering* (Wiley, New York, 2012).
[27] CST MICROWAVE STUDIO™, Version 2014, CST of America, Inc., www.cst.com
[28] S. I. Bozhevolnyi and V. S. Volkov, Appl. Phys. Lett. **79**, 1076 (2001).
[29] T. Holmgaard, Z. Chen, S. I. Bozhevolnyi, L. Markey, A. Dereux, A. V. Krasavin, and A. V. Zayats, Opt. Express **16**, 13585 (2008).